Full-Wave Analysis of a Perfectly Conducting Wire Transmission Line in a Double-Layered Conductor-Backed Medium

NIELS FACHÉ AND DANIËL DE ZUTTER

Abstract—**This paper presents a full-wave eigenmode analysis of a waveguide structure which consists of a double-layered conductor-backed medium with a perfectly conducting cylindrical wire in either the top layer or the bottom layer. The analysis starts with a Fourier series representation of the total longitudinal and transverse current components on the wire surface, which are seen as the sources of the eigenmode of the waveguide. The fields generated by these sources can be expressed in terms of suitable incoming and scattered fields. Finally, Galerkin's method is used to impose the boundary conditions on the wire surface. Numerical results are presented for a typical microwire interconnection structure.**

I. Introduction

In RECENT years much theoretical effort has been invested in the quasi-TEM and full-wave modeling of single and coupled microstrips [1]–[6]. These efforts, combined with experimental verifications of the theoretical models, are justified because of the great importance of the microstrip as an interconnection structure in analog and digital applications.

Another type of interconnection for high-speed applications is the discrete wire technology. Two important applications of this technology are the multiwire and the microwire circuit boards which have become a center of attraction as a new technology for the printed wiring boards [7], [8]. They provide the necessary electrical characteristics to transport high-speed digital signals in very dense circuits.

In this paper a full-wave analysis is presented of a simplified geometrical model of the multiwire and the microwire boards. We suppose that the structure under consideration consists of a double-layered conductor-backed medium. We consider two cases. In the first case the cylindrical wire is located in the bottom layer, i.e., in the substrate. This corresponds to the microwire and multiwire configuration. In the second case the wire is located in the top layer. This corresponds to the wire above ground configuration which is used to model the bond wire in the packaging of high-speed integrated circuits [9].

Manuscript received May 4, 1988; revised October 20, 1988. The first author is supported by a grant from the Instituut tot Aanmoediging van het Wetenschappelijk Onderzoek in Nijverheid en Landbouw. D. De Zutter is a Research Associate of the National Fund for Scientific Research of Belgium.

The authors are with the Laboratory of Electromagnetism and Acoustics, University of Ghent, Sint-Pietersnieuwstraat 41, 9000 Ghent, Belgium.

IEEE Log Number 8825746.

The first purpose of our full-wave analysis is to determine the frequency range in which the structure behaves as a quasi-TEM structure. However, our analysis allows us to calculate the dispersion characteristics of the structure when the latter is used in very high frequency applications.

In contrast to the microstrip analysis, very little work has been done in modeling the multiwire and the microwire structures. To the best of the authors' knowledge, this paper presents the first full-wave analysis of the discrete wire structure. The quasi-TEM analysis has already been performed [10].

II. Geometry of the Problem

The structures under consideration are shown in Fig. 1(a) and (b). They consist of a double-layered lossless medium backed by a perfectly conducting ground plane. Each layer has a permittivity ϵ_{ri} and a permeability μ_{ri}, $i=1, 2$. In the structure of Fig. 1(a) the wire is located in the top layer, while in Fig. 1(b) the wire is located in the substrate. The parameters r_c, d, and H fully specify the geometry of the structure; they are the radius of the wire, the thickness of the substrate, and the distance from the ground plane to the center of the wire, respectively.

III. Overview of the Eigenmode Analysis

We restrict the presentation of our eigenmode theory to the analysis of the structure in Fig. 1(a). The modifications for the case of Fig. 1(b) will be briefly mentioned. As we want to determine an eigenmode of the structure in Fig. 1(a), all field components depend upon x through the common phase factor $\exp(-j\beta x)$, where β represents the propagation constant. The time dependence $\exp(j\omega t)$ is suppressed. The actual electromagnetic fields can be written as

$$\begin{aligned} \boldsymbol{e}(x, y, z) &= \boldsymbol{E}(y, z)\exp(-j\beta x) \\ \boldsymbol{h}(x, y, z) &= \boldsymbol{H}(y, z)\exp(-j\beta x). \end{aligned} \tag{1}$$

The determination of an eigenmode starts from a Fourier series representation of the total longitudinal and transverse current on the wire. From this the *incoming* field, i.e., the field in the top layer in the absence of the substrate, is calculated. As a next step we determine the *scattered* field due to the presence of the substrate. The scattered field is

0018-9480/89/0300-0512$01.00 ©1989 IEEE

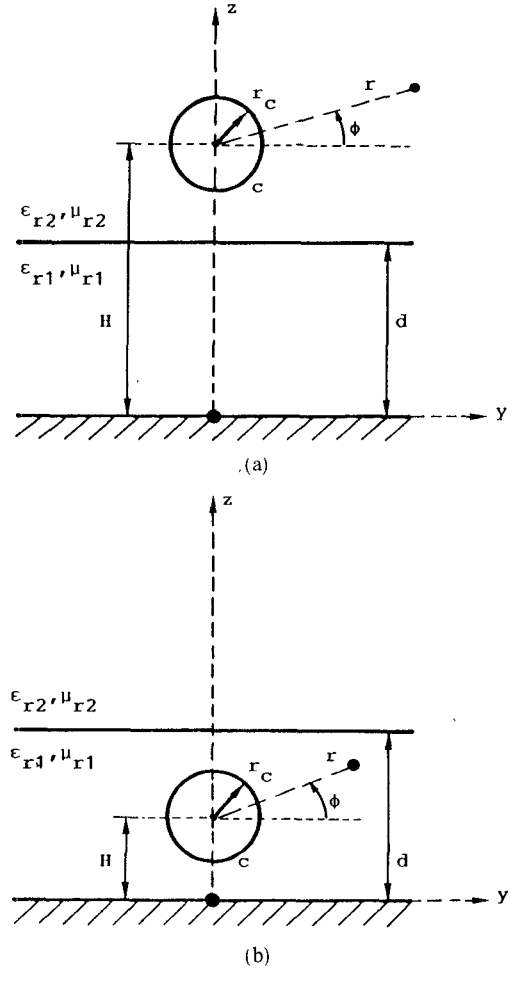

Fig. 1. Cylindrical wire transmission line in a double layered, conductor-backed medium.

first calculated in the spectral domain using a TE–TM mode decomposition [6]. Inverse Fourier transformation yields the scattered field in the spatial domain. Finally, in order to find an eigenmode, we impose the boundary conditions on the surface wire, using Galerkin's method. These different steps in our theory are worked out in the following sections. At the end of each section we briefly describe the modifications for the case of Fig. 1(b).

IV. Incoming Field in the Space and Spectral Domain

The incoming longitudinal fields $E^i_{x,2}$ and $H^i_{x,2}$, i.e., the fields in the top layer in the absence of the substrate, satisfy the following Helmholtz equations:

$$\nabla^2 E^i_{x,2} + \gamma_2^2 E^i_{x,2} = 0$$

$$\nabla^2 H^i_{x,2} + \gamma_2^2 H^i_{x,2} = 0. \tag{2}$$

Here $\gamma_2^2 = k_2^2 - \beta^2$ with $k_2 = k_0 \varepsilon_{r2}\mu_{r2}$ and $k_0 = \omega/c$, while γ_2 itself is defined as the root of γ_2^2 with nonnegative real or nonpositive imaginary part. Starting form (2), the incoming fields can be determined [11] from

$$E^i_{x,2}(r,\phi) = \int_0^{2\pi} G_2 \frac{\partial E_{x,2}(r'=r_c,\phi')}{\partial r'} r_c\, d\phi' \tag{3}$$

$$H^i_{x,2}(r,\phi) = -\int_0^{2\pi} H_{x,2}(r'=r_c,\phi') \frac{\partial G_2}{\partial r'} r_c\, d\phi' \tag{4}$$

where $G_2(\boldsymbol{r}|\boldsymbol{r}') = j/4H_0^{(2)}(\gamma_2|\boldsymbol{r}-\boldsymbol{r}'|)$. The integration is performed over the boundary c of the wire. In (4), $H_{x,2}(r'=r_c,\phi')$ is the as-yet-unknown *total* longitudinal magnetic field on the wire surface, while $\partial E_{x,2}/\partial r(r'=r_c,\phi')$ in (3) represents the derivative with respect to r of the *total* longitudinal electric field on the wire surface. To obtain (3) and (4) we used Green's theorem together with the boundary conditions on the wire; i.e., $E_{x,2}=0$ and $\partial H_{x,2}/\partial r = 0$ on c. As a next step, we expand the unknown functions in the integrands of (3) and (4) in an angular Fourier series:

$$H_{x,2} = \sum_{n=-\infty}^{n=+\infty} A_n \exp(jn\phi')$$

$$\frac{\partial E_{x,2}}{\partial r'} = \sum_{n=-\infty}^{n=+\infty} B_n \exp(jn\phi'). \tag{5}$$

The coefficients A_n and B_n are still unknown. From the series (5) one can directly determine the series expansion for the current components $J_{s,\phi}$ and $J_{s,x}$ on the wire. As a starting point in the determination of the eigenmode equation, the Fourier series in (5) form an equivalent alternative for the Fourier series of the total current components on the wire. Substituting (5) into (3) and (4), the incoming longitudinal fields become

$$E^i_{x,2}(\boldsymbol{r}) = \sum_{n=-\infty}^{n=+\infty} r_c B_n \int_0^{2\pi} G_2 \exp(jn\phi')\, d\phi'$$
$$= \sum_{n=-\infty}^{n=+\infty} C_n H_n^{(2)}(\gamma_2 r) \exp(jn\phi) \tag{6}$$

with

$$C_n = \frac{jr_c\pi}{2} J_n(\gamma_2 r_c) B_n \tag{7}$$

and

$$H^i_{x,2}(\boldsymbol{r}) = -\sum_{n=-\infty}^{n=+\infty} r_c A_n \int_0^{2\pi} \frac{\partial G_2}{\partial r'} \exp(jn\phi')\, d\phi'$$
$$= \sum_{n=-\infty}^{n=+\infty} D_n H_n^{(2)}(\gamma_2 r) \exp(jn\phi) \tag{8}$$

with

$$D_n = -\frac{jr_c\pi}{2} \gamma_2 J_n'(\gamma_2 r_c) A_n. \tag{9}$$

J_n and J_n' represent the Bessel function of the first kind of order n and its derivative, and $H_n^{(2)}$ is the Hankel function of the second kind of order n. The integrals appearing in (6) and (8) are calculated in Appendix I.

If we want to determine the scattered fields due to the presence of the substrate, it will be necessary to introduce

the spatial Fourier transformation of all fields with respect to the lateral y direction. In [6], the present authors introduced a TE–TM decomposition of the Fourier transformed fields. In this decomposition an arbitrary vector $\boldsymbol{W}(k_y, z)$ is characterized by three different numbers W_z, W' and W'':

$$\boldsymbol{W} = W_z \boldsymbol{u}_z + \left[W'\boldsymbol{k} + W''(\boldsymbol{u}_z \times \boldsymbol{k})\right]/\left(\beta^2 + k_y^2\right)$$
$$\boldsymbol{k} = \beta \boldsymbol{u}_x + k_y \boldsymbol{u}_y \quad \text{and} \quad k^2 = \beta^2 + k_y^2. \tag{10}$$

The incoming fields (6) and (8) can be written as the superposition of a TM mode:

$$(E')^i = A_2^i \exp\left[\Gamma_2(z-d)\right]$$
$$(H'')^i = -\left(j\omega\epsilon_0\epsilon_{r2}/\Gamma_2\right) A_2^i \exp\left[\Gamma_2(z-d)\right]$$
$$(E_z)^i = \left(j/\Gamma_2\right) A_2^i \exp\left[\Gamma_2(z-d)\right] \tag{11}$$

and a TE mode:

$$(E'')^i = B_2^i \exp\left[\Gamma_2(z-d)\right]$$
$$(H')^i = \left[\Gamma_2/(j\omega\mu_0\mu_{r2})\right] B_2^i \exp\left[\Gamma_2(z-d)\right]$$
$$(H_z)^i = \left[B_2^i/(\omega\mu_0\mu_{r2})\right] \exp\left[\Gamma_2(z-d)\right] \tag{12}$$

where $\Gamma_2 = (\beta^2 + k_y^2 - k_0^2 N^2)^{1/2} = (k_y^2 - \gamma_2^2)^{1/2}$. A_2^i and B_2^i still have to be determined.

From (10), (11), and (12) the incoming longitudinal fields are found to be

$$E_{x,2}^i = \left[\left(\beta A_2^i - k_y B_2^i\right)/k^2\right] \exp\left[\Gamma_2(z-d)\right] \tag{13}$$

and

$$H_{x,2}^i = \left[\left(\beta b_2 B_2^i + k_y A_2^i/a_2\right)/k^2\right] \exp\left[\Gamma_2(z-d)\right] \tag{14}$$

with

$$a_2 = \Gamma_2/(j\omega\epsilon_0\epsilon_{r2})$$
$$b_2 = \Gamma_2/(j\omega\mu_0\mu_{r2}). \tag{15}$$

Fourier transformation with respect to y in (6) and (8) yields

$$E_{x,2}^i(k_y, z) = \exp\left[\Gamma_2(z-H)\right] e^i(k_y) \tag{16}$$
$$H_{x,2}^i(k_y, z) = \exp\left[\Gamma_2(z-H)\right] h^i(k_y) \tag{17}$$

with

$$e^i = \frac{1}{\Gamma_2} \sum_{n=-\infty}^{n=+\infty} (j/\pi) C_n \left(\frac{\Gamma_2 - k_y}{\Gamma_2 + k_y}\right)^{n/2} \tag{18}$$

$$h^i = \frac{1}{\Gamma_2} \sum_{n=-\infty}^{n=+\infty} (j/\pi) D_n \left(\frac{\Gamma_2 - k_y}{\Gamma_2 + k_y}\right)^{n/2}. \tag{19}$$

Equations (16) and (17) are valid only for $z \leqslant H - r$. The details of the calculation can be found in Appendix II. Comparing (13) and (14) with (16) and (17) finally yields

$$A_2^i = \left(a_h h^i + a_e e^i\right) k^2 \exp\left[-\Gamma_2(H-d)\right]$$
$$B_2^i = \left(b_h h^i + b_e e^i\right) k^2 \exp\left[-\Gamma_2(H-d)\right] \tag{20}$$

with

$$a_h = a_2 k_y/\tau \qquad a_e = a_2 b_2 \beta/\tau$$
$$b_h = a_2 \beta/\tau \qquad b_e = -k_y/\tau \tag{21}$$
$$\tau = k_y^2 + \beta^2 a_2 b_2.$$

For the calculation of the incoming fields in the case of Fig. 1(b), the top layer is replaced by the substrate material. The incoming fields are now defined as the fields due to a cylindrical wire in a semi-infinite homogeneous medium $(\epsilon_{r1}, \mu_{r1})$. Hence in (3), G_2 must be replaced by the Green's function of a semi-infinite space $(\epsilon_{r1}, \mu_{r1})$ with electric wall at $z = 0$, while in (4) G_2 must be replaced with the Green's function of a semi-infinite space $(\epsilon_{r1}, \mu_{r1})$ with a magnetic wall at $z = 0$. Subsequent calculations of the incoming fields are similar to the ones presented for the case of Fig. 1(a).

V. Scattered Field in the Space and Spectral Domain

The knowledge of the incoming field, the continuity of the tangential electric and magnetic field components (E', E'', H', H'') at the dielectric interface, the zero tangential electric field at the ground plane, and only outgoing waves in the top layer yield the TM and TE modes for both the top layer and the substrate. For the TM mode the total fields in both the substrate and the top layer turn out to be:

substrate ($0 < z < d$)

$$E_1' = A_1 \sinh(\Gamma_1 z)$$
$$H_1'' = -\left(j\omega\epsilon_0\epsilon_{r1}/\Gamma_1\right) A_1 \cosh(\Gamma_1 z)$$
$$E_{z,1} = jA_1/\Gamma_1 \cosh(\Gamma_1 z) \tag{22}$$

top layer ($z > d$)

$$E_2' = A_2^{sc} \exp\left[-\Gamma_2(z-d)\right] + A_2^i \exp\left[\Gamma_2(z-d)\right]$$
$$H_2'' = \left(j\omega\epsilon_0\epsilon_{r2}/\Gamma_2\right)\left(A_2^{sc} \exp\left[-\Gamma_2(z-d)\right] - A_2^i \exp\left[\Gamma_2(z-d)\right]\right)$$
$$E_{z,1} = -j/\Gamma_2\left(A_2^{sc} \exp\left[-\Gamma_2(z-d)\right] - A_2^i \exp\left[\Gamma_2(z-d)\right]\right) \tag{23}$$

with

$$A_1 = \frac{2\epsilon_{r2}\Gamma_1 A_2^i}{\epsilon_{r2}\Gamma_1 \sinh(\Gamma_1 d) + \epsilon_{r1}\Gamma_2 \cosh(\Gamma_1 d)} \tag{24}$$

and

$$A_2^{sc} = \frac{\epsilon_{r2}\Gamma_1 \sinh(\Gamma_1 d) - \epsilon_{r1}\Gamma_2 \cosh(\Gamma_1 d)}{\epsilon_{r2}\Gamma_1 \sinh(\Gamma_1 d) + \epsilon_{r1}\Gamma_2 \cosh(\Gamma_1 d)} A_2^i = R_{TM} A_2^i. \tag{25}$$

The TE mode for the two layers is given by:

substrate ($0 < z < d$)

$$E_1'' = B_1 \sinh(\Gamma_1 z)$$
$$H_1' = \left[\Gamma_1/(j\omega\mu_0\mu_{r1})\right] B_1 \cosh(\Gamma_1 z)$$
$$H_{z,1} = \left[B_1/(\omega\mu_0\mu_{r1})\right] \sinh(\Gamma_1 z) \tag{26}$$

top layer ($z > d$)

$$E_2'' = B_2^{sc}\exp\left[-\Gamma_2(z-d)\right] + B_2^{i}\exp\left[\Gamma_2(z-d)\right]$$
$$H_2' = \left[\Gamma_2/(-j\omega\mu_0\mu_{r2})\right]\left(B_2^{sc}\exp\left[-\Gamma_2(z-d)\right] - B_2^{i}\exp\left[\Gamma_2(z-d)\right]\right)$$
$$H_{z,2} = \left[1/(\omega\mu_0\mu_{r2})\right]\left(B_2^{sc}\exp\left[-\Gamma_2(z-d)\right] + B_2^{i}\exp\left[\Gamma_2(z-d)\right]\right) \quad (27)$$

with

$$B_1 = \frac{2\mu_{r1}\Gamma_2 B_2^{i}}{\mu_{r1}\Gamma_2\sinh(\Gamma_1 d) + \mu_{r2}\Gamma_1\cosh(\Gamma_1 d)} \quad (28)$$

and

$$B_2^{sc} = \frac{\mu_{r1}\Gamma_2\sinh(\Gamma_1 d) - \mu_{r2}\Gamma_1\cosh(\Gamma_1 d)}{\mu_{r1}\Gamma_2\sinh(\Gamma_1 d) + \mu_{r2}\Gamma_1\cosh(\Gamma_1 d)} B_2^{i} = R_{TE}B_2^{i}. \quad (29)$$

The superscript sc denotes the scattered field components. The coefficients R_{TM} and R_{TE} are the reflection coefficients for the TM and TE mode, respectively. From (23) and (27) one finds the scattered longitudinal fields:

$$E_{x,2}^{sc} = \left[\left(\beta A_2^{sc} - k_y B_2^{sc}\right)/k^2\right]\exp\left[-\Gamma_2(z-d)\right] \quad (30)$$

$$H_{x,2}^{sc} = \left(j\left[\left(\beta\Gamma_2 B_2^{sc}/(\omega\mu_0\mu_{r2}) - \left(k_y\omega\epsilon_0\epsilon_{r2}/\Gamma_2\right)A_2^{sc}\right)\right]/k^2\right)\exp\left[-\Gamma_2(z-d)\right]. \quad (31)$$

Inverse Fourier transformation yields the scattered longitudinal fields in the top layer in the space domain:

$$E_{x,2}^{sc}(y,z) = \int_{-\infty}^{+\infty}\left[\left(\beta A_2^{sc} - k_y B_2^{sc}\right)/k^2\right] \cdot\exp\left[-\Gamma_2(z-d) - jk_y y\right]dk_y \quad (32)$$

$$H_{x,2}^{sc}(y,z) = \int_{-\infty}^{+\infty} j\left(\beta\Gamma_2/(\omega\mu_0\mu_{r2})B_2^{sc} - k_y\omega\epsilon_0\epsilon_{r2}/\Gamma_2 A_2^{sc}\right)/k^2 \times\exp\left[-\Gamma_2(z-d) - jk_y y\right]dk_y. \quad (33)$$

As a last step before the construction of the eigenvalue matrix we calculate the Fourier series decomposition of the scattered longitudinal field on the boundary c of the wire. For the longitudinal electric field one finds

$$E_{x,2}^{sc} = \sum_{n=-\infty}^{n=+\infty} E_n\exp(jn\phi) \quad (34)$$

with

$$E_n = J_n(\gamma_2 r_c)\int_{-\infty}^{+\infty}\left[\left(\beta R_{TM}a_h - k_y R_{TE}b_h\right)h^{i} + \left(\beta R_{TM}a_e - k_y R_{TE}b_e\right)e^{i}\right] \times(-1)^n\left(\frac{\Gamma_2 - k_y}{\Gamma_2 + k_y}\right)^{n/2}\exp\left[-2\Gamma_2(H-d)\right]dk_y \quad (35)$$

while the longitudinal magnetic field is given by

$$H_{x,2}^{sc} = \sum_{n=-\infty}^{n=+\infty} F_n\exp(jn\phi) \quad (36)$$

with

$$F_n = J_n(\gamma_2 r_c)\int_{-\infty}^{+\infty} j\Big(\left[\beta\Gamma_2 R_{TE}b_h/(\omega\mu_0\mu_{r2}) - k_y\omega\epsilon_0\epsilon_{r2}R_{TM}a_h/\Gamma_2\right]h^{i} + \left[\beta\Gamma_2 R_{TE}b_e/(\omega\mu_0\mu_{r2}) - k_y\omega\epsilon_0\epsilon_{r2}R_{TM}a_e/\Gamma_2\right]e^{i}\Big) \times(-1)^n\left(\frac{\Gamma_2 - k_y}{\Gamma_2 + k_y}\right)^{n/2}\exp\left[-2\Gamma_2(H-d)\right]dk_y. \quad (37)$$

To obtain (35) and (37) we made use of

$$\int_0^{2\pi}\exp\left[j(-n\phi' - k_y y') - \Gamma_2(z'-H)\right]d\phi' = 2\pi(-1)^n\left(\frac{\Gamma_2 - k_y}{\Gamma_2 + k_y}\right)^{n/2}J_n(\gamma_2 a). \quad (38)$$

For the calculation of (38) we refer the reader to Appendix II, eq. (A7), where a similar integral is calculated. The integrals in (35) and (37) must be calculated numerically. The integration interval is divided into three parts: $[-\infty, -k_c]$, $[-k_c, k_c]$, and $[k_c, +\infty]$. The value of k_c is chosen such that Γ_1 and Γ_2 can be approximated by $|k_y|$ while $\beta^2 + k_y^2$ can be replaced by k_y^2 in the first and the third interval. The integration over these intervals is performed using Gauss–Laguerre quadrature formulas. Due to resonant modes of the structure the integrands of (35) and (37) exhibit a finite number of poles in the interval $[-k_c, +k_c]$. To avoid these singularities, the original path along the real k_y axis is replaced by a new path in the complex k_y plane [6]. The integration along this new path is performed using a Gauss quadrature formula.

In contradistinction to the case of Fig. 1(a), where the excitation is a given incoming field in the top layer, the source of the scattered field in the case of Fig. 1(b) is a known incoming field in the substrate which is incident on the top layer. The scattered field is found using a procedure similar to the one used in this section. We emphasize that the scattered field in the substrate must also be required to satisfy the boundary conditions at the perfectly conducting ground plane.

VI. Buildup of the Eigenvalue Matrix

The eigenvector of the structure in Fig. 1(a) is found by expressing the equality between the total longitudinal electric (magnetic) field on the boundary of the wire and the sum of the incoming and the scattered longitudinal electric (magnetic) field. We notice that the total longitudinal electric field is zero on the boundary of the wire. From (6) and (34) the electric boundary condition is expressed by

$$E_n + C_n H_n^{(2)}(\gamma_2 r_c) = 0, \qquad n = 0, \pm 1, \pm 2, \cdots \quad (39)$$

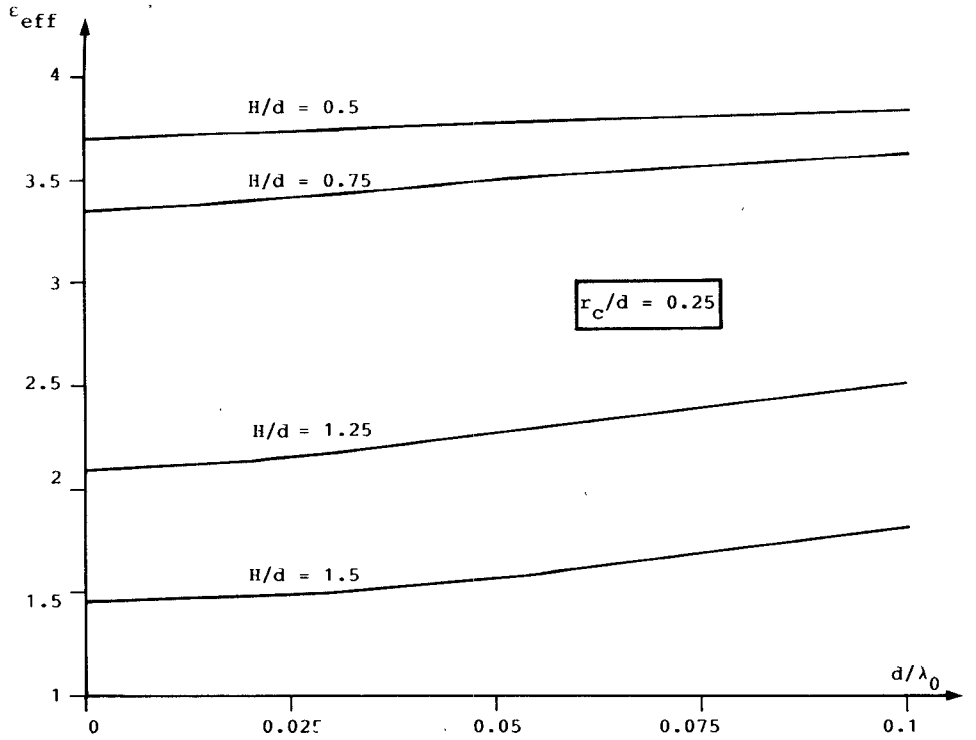

2. Effective dielectric constant as a function of the dimensionless ratio (d/λ_0) for four different positions of the wire in the configuration of Fig. 1 ($r_c/d = 0.25$, $H/d = 0.5, 0.75, 1.25, 1.5$).

while the magnetic boundary conditions from (8) and (36) give

$$F_n + D_n H_n^{(2)}(\gamma_2 r_c) = A_n, \quad n = 0, \pm 1, \pm 2, \cdots. \quad (40)$$

When the Fourier series (5) are restricted to the first $2N+1$ elements ($n = 0, \pm 1, \cdots, \pm N$), eqs. (39) and (40) form a homogeneous set of $4N+2$ equations in $4N+2$ unknowns (A_n, B_n, $n = 0, \pm 1, \cdots, \pm N$) which has only nontrivial solutions for discrete eigenvalues β. These β values are found by using a routine which determines the zeros of a nonlinear function.

In the case of Fig. 1(b) we impose the same boundary conditions at c and arrive at a similar set of eigenvalue equations.

VII. Numerical Results

The main purpose of this paper was the presentation of a full-wave analysis technique for the perfectly conducting wire transmission line in a double-layered conductor-backed medium. Consequently, we restrict the numerical results presented in this section to a single typical discrete wire configuration. In this example the bottom layer is a nonmagnetic dielectric substrate with $\epsilon_r = 4$ while the half-infinite top layer is air ($\epsilon_r = 1$). The ratio of the radius of the cylinder r_c to the thickness of the substrate remains fixed at $r_c/d = 0.25$. Fig. 2 shows the effective dielectric constant as a function of the ratio d/λ_0 (λ_0: wavelength *in vacuo*) for four positions of the cylinder. The position of the cylinder is expressed by the ratio H/d. The four cases we consider are $H/d = 0.5$, 0.75, 1.25, and 1.5. In the first two cases the wire is located in the substrate, while in the last ones the wire is located in the air. In the cases $H/d = 0.75$ and $H/d = 1.25$ the cylinder touches the air–substrate interface. The dispersion is strongest if $H/d = 1.5$. This is a result of the confinement of the electromagnetic field by dielectric guiding of the substrate as the frequency increases. We have checked the accuracy of our results in two ways. The results obtained while changing the number of terms in the Fourier series (5) from 3 ($n = 0, \pm 1$) to more than 3 do not change more than 0.05 percent. As a second check we analyzed the structures considered in [10] in the quasi-TEM ($d/\lambda_0 \to 0$) limit. Within the accuracy with which numerical data can be obtained from the curves printed in [10], our results differ less than 2 percent from the ones in [10].

VIII. Conclusion

This paper presents an analytical technique for the analysis of a perfectly conducting cylindrical wire transmission line in a layered medium. The method is exemplified for a wire in the top layer of a double-layered conductor-backed medium. The modifications for a wire in the substrate are briefly mentioned. The method can be extended to lossy wires either with or without coating and to multilayer structures. The numerical implementation of the technique shows that the angular Fourier series for the total longitudinal magnetic field at the wire and for the radial derivative of the total electric field at the wire, which are the actual starting points for the eigenmode calculations, can be truncated to three terms ($n = 0, \pm 1$ in (39) and (40)) to yield accurate results for the configuration under study. This indicates that our analytical technique leads to an eigenvalue matrix of small dimensions, which can easily be

handled numerically. The numerical results in this paper are restricted to a typical discrete wire structure.

As a next step in our research the characteristic impedance associated with the mode propagating along a wire will be determined and the coupling between wires in a layered medium will be studied in detail. The results will be presented in a forthcoming paper.

Appendix I
Series Expansion of the Incoming Longitudinal Fields

To calculate the integrals in (6) and (8) we use the following addition theorem of the Bessel functions [12]:

$$H_0^{(2)}(\gamma_2|\boldsymbol{r}'-\boldsymbol{r}|) = \sum_{m=-\infty}^{m=+\infty} J_m(\gamma_2 r') H_m^{(2)}(\gamma_2 r) \cdot \exp\left[jm(\phi-\phi')\right]. \quad \text{(A1)}$$

Substitution of (A1) into the integrals of (6) and (8) and interchanging the integration and the summation yields

$$\int_0^{2\pi} G_2 \exp(jn\phi')\, d\phi' = \frac{j\pi}{2} J_n(\gamma_2 r_c) H_n^{(2)}(\gamma_2 r) \exp(jn\phi) \quad \text{(A2)}$$

and

$$\int_0^{2\pi} \frac{\partial G_2}{\partial r'} \exp(jn\phi')\, d\phi' = \frac{j\gamma_2\pi}{2} J_n'(\gamma_2 r_c) H_n^{(2)}(\gamma_2 r) \exp(jn\phi). \quad \text{(A3)}$$

Appendix II
Fourier Transformation of the Incoming Longitudinal Fields

The Fourier transformation of the incident longitudinal field reduces to the Fourier transformation of $H_0^{(2)}(\gamma_2 r)\exp(jn\phi)$. The latter can be done analytically. We define a function $F_n(k_y)$:

$$F_n(k_y) = \frac{1}{2\pi} \int_{-\infty}^{+\infty} J_n(\gamma_2 r_c) H_n^{(2)}(\gamma_2 r) \exp\left[j(n\phi + k_y y)\right] dy. \quad \text{(A4)}$$

Using the addition theorem of Appendix I, the function $F_n(k_y)$ can be rewritten as

$$F_n(k_y) = \frac{1}{(2\pi)^2} \int_{-\infty}^{+\infty} \exp(jk_y y)\, dy \cdot \int_0^{2\pi} H_0^{(2)}(\gamma_2|\boldsymbol{r}'-\boldsymbol{r}|) \exp(jn\phi')\, d\phi'. \quad \text{(A5)}$$

Interchanging the integration order in (A5) and using the Fourier transformation of the Hankel function of the second kind and the zeroth order [13],

$$\int_{-\infty}^{+\infty} H_0^{(2)}(\gamma_2|\boldsymbol{r}'-\boldsymbol{r}|) \exp\left[jk_y(y-y')\right] dy = 2j\frac{\exp(-\Gamma_2|z-z'|)}{\Gamma_2} \quad \text{(A6)}$$

we finally arrive at

$$F_n(k_y) = 2j\frac{\exp\left[\Gamma_2(z-H)\right]}{(2\pi)^2\Gamma_2} \cdot \int_0^{2\pi} \exp\left[j(n\phi' + k_y y') - \Gamma_2(z'-H)\right] d\phi', \quad z < z'. \quad \text{(A7)}$$

To perform the integration over ϕ' we use the following generating function of the Bessel functions and series associated with it [13]:

$$\exp(jz\sin\theta) = \sum_{m=-\infty}^{m=+\infty} \exp(jm\theta) J_m(z) \quad \text{(A8)}$$

where z is an arbitrary complex number. This series expansion is applied to $\exp(-jk_y y')$ and $\exp[-\Gamma_2(z'-H)]$:

$$\exp(jk_y y') = \exp(jr_c k_y \cos\phi') = \sum_{m=-\infty}^{m=+\infty} j^m \exp(-jm\phi') J_m(k_y r_c)$$

$$\exp\left[-\Gamma_2(z'-H)\right] = \exp(-r_c\Gamma_2\sin\phi') = \sum_{k=-\infty}^{k=+\infty} \exp(jk\phi') J_k(jr_c\Gamma_2). \quad \text{(A9)}$$

Inserting (A9) into (A7) enables us to perform the integration over ϕ' in (A9):

$$\int_0^{2\pi} \exp\left[j(n\phi' + k_y y') - \Gamma_2(z'-H)\right] d\phi' = 2\pi \sum_{m=-\infty}^{m=+\infty} j^m J_m(k_y r_c) J_{m-n}(jr_c\Gamma_2). \quad \text{(A10)}$$

Finally, the series in (A10) is written in closed form using another addition theorem for the Bessel functions [13]:

$$\left(\frac{z_1 - z_2\exp(-j\theta)}{z_1 - z_2\exp(+j\theta)}\right)^{\nu/2} J_\nu(w) = \sum_{n=-\infty}^{n=+\infty} J_n(z_2) J_{n+\nu}(z_1) \exp(jn\theta)$$

$$w = \left(z_1^2 + z_2^2 - 2z_1 z_2\cos\theta\right)^{1/2} = \left(\left[z_1 - z_2\exp(-j\theta)\right]\left[z_1 - z_2\exp(j\theta)\right]\right)^{1/2} \quad \text{(A11)}$$

with z_1 and z_2 two arbitrary complex arguments and ν an arbitrary complex number. Using (A11), (A10) leads to

$$\int_0^{2\pi} \exp\left[j(n\phi' + k_y y') - \Gamma_2(z'-H)\right] d\phi' = 2\pi\left(\frac{\Gamma_2 - k_y}{\Gamma_2 + k_y}\right)^{n/2} J_n(\gamma_2 a). \quad \text{(A12)}$$

Applying (A12) in (A7) yields the final expression for $F_n(k_y)$:

$$F_n(k_y) = j\frac{\exp\left[\Gamma_2(z-H)\right]}{\pi\Gamma_2}\left(\frac{\Gamma_2 - k_y}{\Gamma_2 + k_y}\right)^{n/2} J_n(\gamma_2 r_c). \quad \text{(A13)}$$

As $J_n(\gamma_2 r_c)$ is a constant, (A13) and (A4) immediately lead

to the final result we searched for, i.e.,

$$\frac{1}{2\pi}\int_{-\infty}^{+\infty} H_n^{(2)}(\gamma_2 r)\exp\left[j(n\phi + k_y y)\right] dy = j\frac{\exp\left[\Gamma_2(z-H)\right]}{\pi\Gamma_2}\left(\frac{\Gamma_2 - k_y}{\Gamma_2 + k_y}\right)^{n/2}. \quad \text{(A14)}$$

References

[1] R. H. Jansen and M. Kirschning, "Arguments and an accurate model for the power–current formulation of microstrip characteristic impedance," *Arch. Elek. Übertragung.*, Band 37, Heft 3/4, pp. 108–112, 1983.

[2] W. J. Getsinger, "Measurement and modeling of the apparent characteristic impedance of microstrip," *IEEE Trans. Microwave Theory Tech.*, vol. MTT-31, pp. 624–632, Aug. 1983.

[3] Y. Fukuoka, Q. Zhang, D. Neikirk, and T. Itoh, "Analysis of multilayer interconnection lines for a high-speed digital integrated circuit," *IEEE Trans. Microwave Theory Tech.*, vol. MTT-33, pp. 527–532, June 1985.

[4] R. H. Jansen, "The spectral domain approach for microwave integrated circuits," *IEEE Trans. Microwave Theory Tech.*, vol. MTT-33, pp. 1043–1056, Oct. 1985.

[5] M. Kobayashi and F. Ando, "Dispersion characteristics of open microstrip lines," *IEEE Trans. Microwave Theory Tech.*, vol. MTT-35, pp. 101–105, Feb. 1987.

[6] N. Faché and D. De Zutter, "Rigorous full wave space domain solution for dispersive microstrip lines," *IEEE Trans. Microwave Theory Tech.*, vol. 36, pp. 731–737, Apr. 1988.

[7] E. Sugita and O. Ibaragi, "Reliable multiwire circuits with small gauge wires," *IEEE Trans. Components, Hybrids, Manuf. Technol.*, vol. CHMT-2, pp. 532–536, Dec. 1979.

[8] G. Messner, "Cost–density analysis of interconnections," *IEEE Trans. Components, Hybrids, Manuf. Technol.*, vol. CHMT-10, pp. 143–151, June 1987.

[9] C. J. Stanghan and B. M. Macdonal, "Electrical characterization of packages for high-speed integrated circuits," *IEEE Trans. Components, Hybrids, Manuf. Technol.*, vol. CHMT-8, pp. 468–473, Dec. 1985.

[10] H. Shibata and R. Terakado, "Characteristics of transmission lines with a single wire for a multiwire circuit board," *IEEE Trans. Microwave Theory Tech.*, vol. MTT-32, pp. 360–364, Apr. 1984.

[11] A. J. Poggio and E. K. Miller, "Integral equation solutions of three-dimensional scattering problems," in *Computer Techniques for Electromagnetics*. Oxford: Pergamon Press, 1973, pp. 159–261.

[12] W. Magnus, F. Oberhettinger, and R. P. Soni, *Formulas and Theorems for the Special Functions of Mathematical Physics*, 3rd ed. Berlin: Springer Verlag, 1966.

[13] G. N. Watson, *Theory of Bessel Functions*, 2nd ed. Cambridge: Cambridge University Press, 1962.

✠

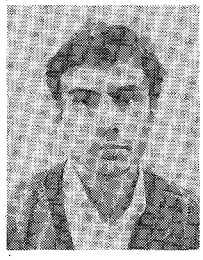

Niels Faché was born in Ghent, Belgium, on July 4, 1964. He received the degree in electrical engineering from the University of Ghent in 1986. He is currently working toward the Ph.D. degree in electrical engineering at the University of Ghent, where his research focuses on the electromagnetic modeling of microwave interconnections.

✠

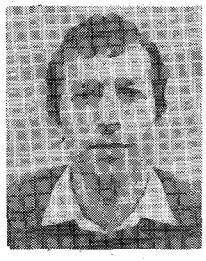

Daniël De Zutter was born in Eeklo, Belgium, on November 8, 1953. He received the degree of electrical engineer from the University of Ghent, Ghent, Belgium, in 1976. From September 1976 to September 1984 he was a research and teaching assistant at the Laboratory of Electromagnetism and Acoustics (LEA) of the same university. In October 1981 he obtained the Ph.D. degree from that university and in the spring of 1984 he completed a thesis leading to a degree equivalent to the French "Aggrégation" or the German "Habilitation."

Most of his scientific work has dealt with the electrodynamics of moving media, with emphasis on the Doppler effect and the forces involved in the interaction of fields with moving media. At present he is with the LEA as a Research Associate of the National Fund for Scientific Research of Belgium. His major research topics are hyperthermia, in particular the field calculations inside biological tissues, the electrodynamics of moving media applied to magnetic levitation and suspension, and the propagation characteristics of high-frequency interconnections.